Structural and Electronic Properties of the Noncubic Superconducting Fullerides A'_4C_{60} (A' = Ba, Sr)

Craig M. Brown,[1,2] Susumu Taga,[3] Balvinder Gogia,[4] Konstantinos Kordatos,[1] Serena Margadonna,[1] Kosmas Prassides,[1] Yoshihiro Iwasa,[3] Katsumi Tanigaki,[5] Andrew N. Fitch,[6] and Philip Pattison[7]
[1]*School of Chemistry, Physics and Environmental Science, University of Sussex, Brighton, BN1 9QJ, United Kingdom*
[2]*Institut Laue Langevin, B.P. 156, F-38042 Grenoble, France*
[3]*Japan Advanced Institute of Science and Technology, Tatsunokuchi, Ishikawa 923-1292, Japan*
[4]*Department of Advanced Chemical Technology, National Institute of Materials and Chemical Technology, 1-1 Higashi, Tsukuba, Ibaraki 305-8565, Japan*
[5]*Faculty of Science, Osaka-city University, PREST, JST. 3-3-138 Sugimoto, Sumiyoshi-ku, Osaka 558-8585, Japan*
[6]*European Synchrotron Radiation Facility, B.P. 220, F-38043 Grenoble, France*
[7]*Institute of Crystallography, University of Lausanne, CH-1015 Lausanne, Switzerland*
(Received 23 April 1999)

The absence of superconductivity in noncubic alkali fullerides, A_4C_{60} (A = K, Rb, Cs) has been associated with the effects of electron correlation and electron-phonon interaction on the narrow t_{1u}-derived conduction band. We find that the structurally related alkaline earth fullerides, A'_4C_{60} (A' = Sr, Ba), are superconducting with small values of the densities of states at the Fermi level, N_{ϵ_F}. Close contacts between Ba^{2+} ions and neighboring C_{60} units in Ba_4C_{60} imply a strong orbital hybridization, which is evidently responsible for stabilizing the noncubic superconducting phase, in contrast to insulating A_4C_{60}.

PACS numbers: 74.70.Wz, 61.10.Nz, 61.48.+c

Alkali fullerides with stoichiometry A_3C_{60} are superconducting with critical temperatures, T_c at ambient pressure as high as 33 K [1]. They invariably adopt cubic structures with their conduction band derived from the t_{1u} levels of C_{60} and superconductivity encountered only close to half filling [2]. For other stoichiometries and levels of band filling, a variety of structural, electronic, and magnetic instabilities to insulating states is encountered and the metallic (and superconducting) state is suppressed [1]. Little systematic investigation of the properties of other fulleride families, like those of the alkaline earth metals, has been undertaken. The primary reason for this has been the difficulty associated with the synthesis of phase-pure samples. However, due to the divalent character of these elements, the t_{1u}-derived band is now full, and occupation of the (LUMO + 1) t_{1g}-derived states occurs, opening the way to different energy scales and different criteria for the occurrence of superconductivity. Early work reported the occurrence of superconductivity in Ba-doped C_{60} systems with $T_c = 6.5$ K. The composition of the superconducting phase was originally established as Ba_6C_{60} with a body centered cubic structure (space group $Im\bar{3}$) [3]. Subsequent work provided evidence that the true superconducting phase in this system may not have the composition Ba_6C_{60}, but rather Ba_4C_{60} with an orthorhombic structure [4]. However, synthetic difficulties meant that Ba_4C_{60} could be obtained only as a minority phase and the question concerning the nature and structural and electronic properties of the superconducting Ba-C_{60} phase remained unresolved. As the fullerene superconductors identified so far have been limited to cubic or slightly distorted cubic structures, the work by Baenitz *et al.* [4] raised serious questions about the structural criteria for fullerene superconductors. The identification of the superconducting phase in the Ba-C_{60} phase field thus becomes of significant importance for the understanding of fullerene superconductivity.

We have recently reported the synthesis and structural and electronic characterization of A'_6C_{60} (A' = Ba, Sr) [5]. Both phases are metallic, but importantly not superconducting. In this paper, we present the synthesis of high quality A'_4C_{60} (A' = Ba, Sr) samples and establish unambiguously by SQUID measurements the nature of the bulk superconducting phases in the Ba-C_{60} and Sr-C_{60} systems. We also report the crystallographic characterization of the Ba_4C_{60} superconductor by synchrotron x-ray powder diffraction in the temperature range 5–295 K. This reveals a highly anisotropic orthorhombic structure (space group *Immm*) which shows no thermal expansion along the short orthorhombic c axis, signature of strong hybridization between metal and carbon orbitals. In sharp contrast to the alkali fulleride phases, superconductivity in alkaline earth fullerides is encountered away from nominal half filling of the t_{1g}-derived band and for noncubic crystal structures.

The A'_4C_{60} (A' = Ba, Sr) samples were prepared by reaction of stoichiometric quantities of C_{60} and Ba or Sr metals (99.9% pure) in tantalum cells inside sealed quartz tubes at 2×10^{-6} Torr. Annealing was carried out between 550 and 650 °C for 12 days with intermittent grindings. Phase purity was monitored by powder x-ray diffraction and SQUID magnetometry. At the end of the annealing period, the superconducting fraction at 2 K increased to 17% for A'_4C_{60}, while it decreased to

 0031-9007/99/83(11)/2258(4)$15.00

<1% for nominal $A_6'C_{60}$ with a well-defined peak for $A_x'C_{60}$ at $x = 4$. At the same time, this is accompanied by the growth of the diffraction peaks of $A_4'C_{60}$. These results unambiguously showed that the superconducting phase has the composition $A_4'C_{60}$ rather than $A_6'C_{60}$. SQUID measurements were performed on 50-mg samples sealed in quartz tubes in the temperature range 2–350 K with a quantum design SQUID magnetometer (MPMS 7T). Total susceptibilities were obtained from the difference of the values measured at 4 and 2 T in order to remove ferromagnetic impurities present. High-resolution synchrotron x-ray powder diffraction data on a Ba_4C_{60} sample sealed in a 0.5-mm diameter glass capillary were collected in continuous scanning mode using nine Ge(111) analyzer crystals on the BM16 beam line at the European Synchrotron Radiation Facility (ESRF), Grenoble, France at 295 K ($\lambda = 0.84884$ Å). Data were rebinned in the 2θ range 4°–70° to a step of 0.005°. Low temperature diffraction measurements at 5 and 10 K were performed on the same capillary on the BM1B beam line at the ESRF with a continuous flow He cryostat (Janis Inc.), equipped with a rotating sample stick ($\lambda = 0.79930$ Å). Data were collected in the 2θ range 4.8°–51.0° at a step of 0.01° using a Si(111) analyzer crystal. Data analysis was performed with the GSAS suite of powder diffraction programs [6].

The inset in Fig. 1 shows the results of the magnetic measurements at 10 G [zero-field cooling (ZFC) conditions] for Ba_4C_{60} and Sr_4C_{60}. Diamagnetic shielding is evident, signaling superconducting transitions at 6.7 and 4.4 K for Ba_4C_{60} and Sr_4C_{60}, respectively. Figure 1 also shows the results obtained at high magnetic fields. The temperature dependence of the susceptibility, χ was described well by including a Curie $1/T$ (arising from lattice defects) and a temperature independent term. The latter comprises both paramagnetic (Pauli spin susceptibility, χ_P) and diamagnetic (core, χ_c and Landau, χ_L contributions) terms. Values of χ_P were extracted as 5.5×10^{-4} and 2.2×10^{-4} emu/mol for Ba_4C_{60} and Sr_4C_{60}, respectively, following the procedure of Ref. [5]. Using the expression, $\chi_P = 2\mu_B^2 N_{\epsilon_F}$, N_{ϵ_F} can then be determined as 6.0 and 2.5 states eV^{-1} $(\text{mol } C_{60})^{-1}$ for Ba_4C_{60} and Sr_4C_{60}, respectively.

Inspection of the synchrotron x-ray powder diffraction profile of Ba_4C_{60} at 295 K (Fig. 2) shows that the majority of reflections index to orthorhombic symmetry. However, some reflections could not be accounted for. By comparison to diffraction data of single phase Ba_6C_{60} ($a = 11.20$ Å) and Ba_3C_{60} ($a = 11.34$ Å), we assign these to small fractions of these two phases. Rietveld refinements were then performed by taking into account the coexistence of three phases and using the structural models of Ba_6C_{60} [3] and Ba_3C_{60} (space group $Pm\overline{3}n$) [7]. The starting structural model of Ba_4C_{60} was derived from that of the A_4C_{60} ($A = \text{K, Rb}$) systems. These adopt a tetragonal structure in which the C_{60} units are merohedrally disordered about the [001] axis and the alkali ions reside in distorted tetrahedral sites (space group $I4/mmm$) [8]. The orthorhombic unit cell of Ba_4C_{60} then necessitates orientational ordering of the C_{60} units and two inequivalent barium sites, in analogy with Cs_4C_{60} [9]. After aligning the twofold axis of C_{60} with the

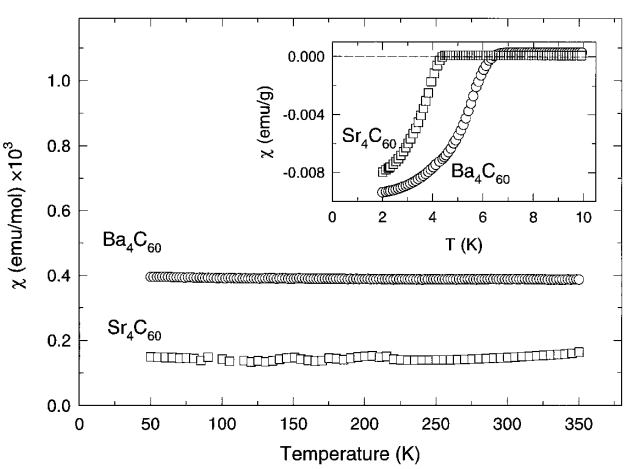

FIG. 1. Temperature dependence of the magnetic susceptibilities of Ba_4C_{60} and Sr_4C_{60}. The inset shows the susceptibilities measured under ZFC conditions in a field of 10 G.

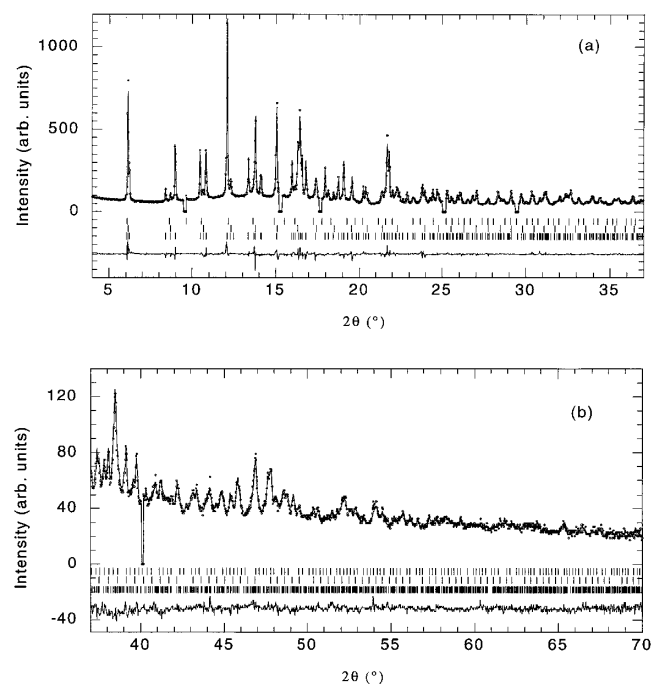

FIG. 2. Final observed (points) and calculated (solid line) synchrotron x-ray powder diffraction profiles for Ba_4C_{60} at 295 K in the range 4° to 70° ($\lambda = 0.848\,84$ Å). The lower panels show the difference profiles and the ticks mark the positions of the Bragg reflections of Ba_4C_{60} [majority phase: 86.1(2)%, lower most], Ba_6C_{60} [minority phase: 11.8(1)%, middle], and Ba_3C_{60} [minority phase: 2.1(1)% upper most]. Some sharp peaks originating from a nonfulleride phase were excluded from the refinement.

crystallographic b axis, the space group is *Immm* if body centering is retained (in analogy to Ba_6C_{60}) or *Pnnm* if the C_{60} unit at $(0.5, 0.5, 0.5)$ is rotated by 90° about the c axis (in analogy to Ba_3C_{60}). The two C_{60} units in the unit cell were then allowed to rotate anticlockwise in steps of 5° between 0° and 90° about the [100], [010], and [001] directions for both models and the agreement factor χ^2 was monitored. In the course of these refinements, the C_{60} molecular geometry was kept fixed with all C-C bonds at 1.44 Å, while all instrumental parameters were constrained to the values obtained by the LeBail pattern decomposition technique. A deep minimum in χ^2 ($\approx$6.8) results for both models for the starting orientation, in which the hexagon-hexagon (6:6) C-C bond is aligned along the b axis.

Final Rietveld refinements were performed by using this C_{60} orientation for both *Immm* and *Pnnm* space groups. The C_{60} anions in Ba_4C_{60} and Ba_6C_{60} (but not in Ba_3C_{60}) were allowed to dilate radially, while preserving the I_h molecular symmetry. For Ba_4C_{60}, the C-C bond lengths refined to 1.436(4) Å and the bond angles in the pentagonal faces to 108.000(8)° and in the hexagonal faces to 120.06(9)°. The positional parameters of the two inequivalent barium ions in Ba_4C_{60} at $(0.5, y, 0)$ and $(x, 0.5, 0)$ and of the barium ion in Ba_6C_{60} at $(x, 0, 0.5)$ were also refined. An improvement in the refinement was evident when anisotropic temperature factors were used and refined for Ba^{2+} in Ba_4C_{60}. Finally, the peak shape was described by the asymmetry function of Finger *et al.* [10]. The fractions of the three phases converged to 86.1(2)% for Ba_4C_{60}, 11.8(1)% for Ba_6C_{60}, and 2.1(1)% for Ba_3C_{60}. The final result of the refinement at 295 K using the *Immm* structural model for Ba_4C_{60} is shown in Fig. 2 [agreement factors, $R_{wp} = 5.3\%$, $R_{exp} = 2.6\%$; $a = 11.6101(2)$ Å, $b = 11.2349(2)$ Å, $c = 10.8830(2)$ Å] with the fitted parameters summarized in Table I. We also explored in detail the *Pnnm* structural model for Ba_4C_{60}. The refinement proved unstable and no atomic parameters could be varied. This instability together with the absence of any reflections violating body centering extinctions rule out the *Pnnm* model.

The diffraction profiles of Ba_4C_{60} measured at 5 and 10 K showed no evidence for a structural phase transition on cooling. Rietveld refinements proceeded routinely with the same *Immm* structural model (5 K: agreement factors, $R_{wp} = 8.3\%$, $R_{exp} = 5.8\%$; cell constants, $a = 11.6008(5)$ Å, $b = 11.1841(5)$ Å, $c = 10.8836(5)$ Å. 10 K: agreement factors, $R_{wp} = 9.6\%$, $R_{exp} = 7.1\%$; cell constants, $a = 11.6016(5)$ Å, $b = 11.1843(5)$ Å, $c = 10.8837(5)$ Å). It is evident that orthorhombic Ba_4C_{60} is strongly anisotropic with negligible thermal expansivity along the short c axis, reminiscent of polymerized AC_{60} [11] and Na_2AC_{60} [12] fullerides in which there are bridging C-C bonds between the C_{60} anions. As no evidence for such type of bonding is present in Ba_4C_{60}, the origin of the severe anisotropy in thermal expansion [$\delta a/a = 0.080(6)\%$, $\delta b/b = 0.454(6)\%$, and $\delta c/c = -0.006(7)\%$ between 5 and 295 K] may be sought in the diverse character of Ba^{2+}-C bonding interactions.

A perspective view of the orthorhombic structure of Ba_4C_{60} is shown in Fig. 3. Compared to the bcc unit cell of Ba_6C_{60}, it arises from ordering of Ba^{2+} vacancies in the [100] and [010] planes, leading to lattice contraction along the c axis. Both crystallographically distinct Ba^{2+} ions in the unit cell have identical coordination environment, namely they lie directly above the centers of two hexagonal and two pentagonal faces of neighboring C_{60} anions. In both cases, the average Ba-C distances are

TABLE I. Refined parameters for orthorhombic Ba_4C_{60} obtained from Rietveld refinement of the synchrotron x-ray powder diffraction data at 295 K (space group *Immm*, $R_{wp} = 5.3\%$, $R_{exp} = 2.6\%$). The cell constants are $a = 11.6101(2)$, $b = 11.2349(2)$, and $c = 10.8830(2)$ Å, and the weight fraction of the Ba_4C_{60} phase is 86.1(2)%. The weight fractions of the minority phases, Ba_6C_{60} and Ba_3C_{60} are 11.8(1)% and 2.1(1)%, respectively. The cell constants of cubic Ba_6C_{60} (space group $Im\bar{3}$) and Ba_3C_{60} (space group $Pm\bar{3}n$) are 11.1959(2) and 11.338(1) Å, respectively.

Atom	x/a	y/b	z/c	$B_{iso}/Å^2$ ($\beta_{11}, \beta_{22}, \beta_{33}$)
Ba(1)	0.5	0.2034(2)	0.0	1.9(1), 2.9(2), 0.9(1)
Ba(2)	0.2488(1)	0.5	0.0	2.7(1), 3.7(2), 0.6(1)
C(11)	0.3005(2)	0.0	0.0652(1)	0.16(8)
C(12)	0.0	−0.063 88(4)	0.3206(2)	0.16(8)
C(13)	0.10014(6)	−0.127 86(7)	0.2798(2)	0.16(8)
C(21)	0.2003(1)	−0.63 88(4)	0.2389(1)	0.16(8)
C(22)	0.12373(7)	−0.271 0(2)	0.106 82(6)	0.16(8)
C(23)	0.06187(4)	−0.310 5(2)	0.0	0.16(8)
C(31)	0.2240(2)	−0.207 0(1)	0.066 00(3)	0.16(8)
C(32)	0.06187(4)	−0.231 4(1)	0.213 7(1)	0.16(8)
C(33)	0.2622(2)	−0.103 45(6)	0.131 99(8)	0.16(8)

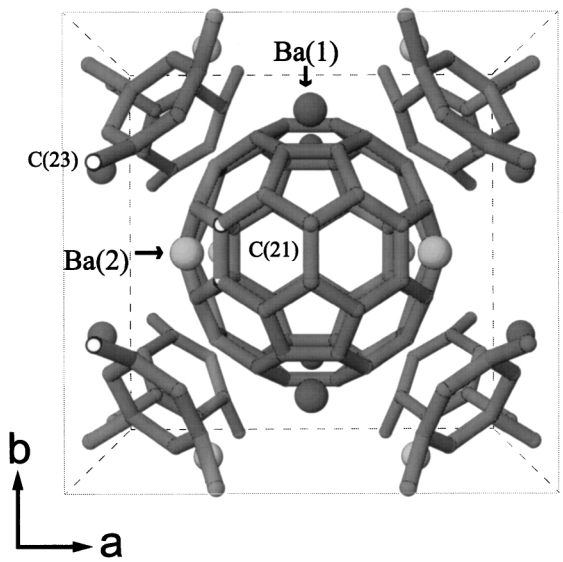

FIG. 3. Projection of the body centered orthorhombic structure of Ba_4C_{60} on the [110] basal plane. The two sets of crystallographically distinct barium ions, Ba(1) ($m2m$ site) and Ba(2) ($2mm$ site) are depicted as dark and light grey spheres, respectively. The hexagon C(21) and pentagon C(23) atoms which are in close contact to Ba(2) are depicted as white spheres.

comparable, 3.29(2) Å for Ba(1) and 3.26(17) Å for Ba(2) at 295 K. However, while the Ba(1) site adopts quite a regular coordination with only a slight displacement from the hexagon and pentagon ring centroids (tilt angles from ring normals are 1.1° in both cases), the Ba(2) site is very irregular with large displacements from the two ring centroids (with tilt angles of 15.3° and 9.5°, respectively). Moreover, the shortest Ba(2)-C contacts are very small: 2.990(4) Å and 3.040(3) Å to hexagon C(21) and pentagon C(23) atoms, respectively. These are smaller than the sum of the ionic radius of Ba^{2+} (1.35 Å) and the van der Waals radius of C (1.70 Å), implying strong hybridization between the $5d$ orbitals of Ba(2) and the $2p$ orbitals of carbon. The coordination geometry of the two Ba^{2+} ions is retained on cooling to 10 and 5 K. Ba(1) remains regularly coordinated with all Ba-C contacts larger than 3.25 Å, while Ba(2) is again sterically crowded with unchanged shortest Ba(2)-C contacts at 5 K of 2.983(3) Å and 3.044(6) Å to C(21) and C(23) atoms, respectively.

The occurrence of superconductivity in noncubic Ba_4C_{60} is in sharp contrast with the absence of superconductivity in alkali fullerides, A_4C_{60} ($A = \mathrm{K, Rb, Cs}$), despite the similar or identical structures. In A_4C_{60}, the electrons are localized, most likely by the combined effect of electron correlation and electron-phonon interaction [13]. Since the alkali fullerides are at the verge of the metal-insulator boundary, because of the narrow band nature of the t_{1u}-originated conduction band, distortion from cubic symmetry and deviation from half filling easily destroy the metallic state and, as a result, superconductivity. In $A_4'C_{60}$, the metallic state seems to be much more robust. In fact, N_{ϵ_F}, determined by magnetic susceptibility measurements is 6.0 and 2.5 states eV^{-1} (mol $C_{60})^{-1}$ for Ba_4C_{60} and Sr_4C_{60}, respectively. These values are considerably smaller than those of the t_{1u}-superconductors, K_3C_{60} and Rb_3C_{60}, indicating broader conduction bands for the $A_4'C_{60}$ systems. Such low N_{ϵ_F} values have been also reported for the nonavalent $A_3Ba_3C_{60}$ system, which is another t_{1g}-superconductor [14].

The low density of states in $A_4'C_{60}$ may be attributed to the hybridization of Ba $5d$ and C_{60} t_{1g} orbitals. The short Ba-C contacts revealed by the structural analysis are strongly suggestive of such orbital mixing. We also conjecture that the broad conduction bands observed in alkaline earth fullerides are attributable to this hybridization effect. In contrast to the alkali fullerides whose metallic state suffers from various instabilities to insulating states, the increased bandwidth in alkaline earth fullerides suppresses such instabilities, leading to the stabilization of the metallic state and the occurrence of superconductivity.

Support by the British Council through a UK/Japan Collaborative Research Grant (CRP) is gratefully acknowledged. Work in Japan was partly supported by the JSPS "Future Program," RFTF96P00104. We thank the ESRF and the Swiss National Science Foundation for provision of synchrotron x-ray beam time.

[1] O. Gunnarsson, Rev. Mod. Phys. **69**, 575 (1997); K. Prassides, Curr. Opin. Solid State Mater. Sci. **2**, 433 (1997); M. J. Rosseinsky, Chem. Mater. **10**, 2665 (1998).
[2] T. Yildirim *et al.*, Phys. Rev. Lett. **77**, 167 (1997); M. Kosaka *et al.*, Phys. Rev. B **59**, R6628 (1999).
[3] A. R. Kortan *et al.*, Nature (London) **360**, 566 (1992).
[4] M. Baenitz *et al.*, Solid State Commun. **96**, 539 (1995); M. Kraus *et al.*, Fullerene Sci. Technol. **3**, 115 (1995).
[5] B. Gogia *et al.*, Phys. Rev. B **58**, 1077 (1998).
[6] A. C. Larsen and R. B. von Dreele, GSAS software, Los Alamos National Laboratory Report No. LAUR 86-748.
[7] A. R. Kortan *et al.*, Phys. Rev. B **47**, 13 070 (1993).
[8] O. Zhou and D. E. Cox, J. Phys. Chem. Solids **53**, 1373 (1992); C. A. Kuntscher, G. M. Bendele, and P. W. Stephens, Phys. Rev. B **55**, R3366 (1997).
[9] P. Dahlke, P. F. Henry, and M. J. Rosseinsky, J. Mater. Chem. **8**, 1571 (1998).
[10] L. W. Finger, D. E. Cox, and A. P. Jephcoat, J. Appl. Crystallogr. **27**, 892 (1994).
[11] P. W. Stephens *et al.*, Nature (London) **370**, 636 (1994).
[12] K. Prassides *et al.*, J. Am. Chem. Soc. **119**, 834 (1997); G. M. Bendele *et al.*, Phys. Rev. Lett. **80**, 736 (1998).
[13] M. Knupfer and J. Fink, Phys. Rev. Lett. **79**, 2714 (1997).
[14] Y. Iwasa *et al.*, Phys. Rev. B **57**, 13 395 (1998).